




The protein corona suppresses the cytotoxic and pro-inflammatory response in lung epithelial cells and macrophages upon exposure to nanosilica

Regina Leibe¹ · I-Lun Hsiao^{1,2} · Susanne Fritsch-Decker¹ · Ulrike Kielmeier¹ · Ane Marit Wagbo¹ · Benjamin Voss¹ · Annemarie Schmidt¹ · Sarah Dorothea Hessman¹ · Albert Duschl³ · Gertie Janneke Oostingh⁴ · Silvia Diabaté¹  · Carsten Weiss¹

Received: 7 November 2018 / Accepted: 28 February 2019 / Published online: 5 March 2019
© Springer-Verlag GmbH Germany, part of Springer Nature 2019

Abstract

Engineered amorphous silica nanoparticles (nanosilica) are one of the most abundant nanomaterials and are widely used in industry. Furthermore, novel nanosilica materials are promising theranostic tools for biomedicine. However, hazardous effects of nanosilica especially after inhalation into the lung have been documented. Therefore, the safe development of nanosilica materials urgently requires predictive assays to monitor toxicity. Here, we further investigate the impact of the protein corona on the biological activity of two different types of nanosilica (colloidal and pyrogenic) in lung cells. As previously described, adsorption of serum proteins to the nanosilica surface suppresses cytotoxicity in macrophages and lung epithelial cells. As the increase of pro-inflammatory mediators is a hallmark of inflammation in the lung upon nanosilica exposure, we studied the potential coupling of the cytotoxic and pro-inflammatory response in A549 human lung epithelial cells and RAW264.7 mouse macrophages. Indeed, cytotoxicity precedes the onset of pro-inflammatory gene expression and cytokine release as exemplified for IL-8 in A549 cells and TNF-alpha in RAW264.7 macrophages after exposure to 0–100 µg/mL nanosilica in medium without serum. Formation of a protein corona not only inhibited cellular toxicity, but also the pro-inflammatory response. Of note, uptake of nanosilica into cells was negligible in the absence, but enhanced in the presence of a protein corona. Hence, the prevailing explanation that the protein corona simply interferes with cellular uptake thus preventing adverse effects needs to be revisited. In conclusion, for the reliable prediction of adverse effects of nanosilica in the lung, *in vitro* assays should be performed in media not complemented with complete serum. However, in case of different exposure routes, e.g., injection into the blood stream as intended for biomedicine, the protein corona prevents acute toxic actions of nanosilica.

Keywords Nanoparticle · Silica · Lung cells · Cell death · Inflammation · Protein corona · Nano–bio-interface

Electronic supplementary material The online version of this article (<https://doi.org/10.1007/s00204-019-02422-9>) contains supplementary material, which is available to authorized users.

✉ Silvia Diabaté
silvia.diabate@kit.edu

✉ Carsten Weiss
carsten.weiss@kit.edu

¹ Institute of Toxicology and Genetics, Karlsruhe Institute of Technology, Hermann-von-Helmholtz-Platz 1, 76344 Eggenstein-Leopoldshafen, Germany

Introduction

The production volume of amorphous silica nanoparticles (NPs) is one of the largest among the manufactured nanomaterials worldwide with several million tons and wide

² School of Food Safety, College of Nutrition, Taipei Medical University, 250 Wuxing St., Taipei 11031, Taiwan

³ Department of Biosciences, Allergy Cancer BioNano Research Centre (ACBN), University of Salzburg, Hellbrunnerstraße 34, 5020 Salzburg, Austria

⁴ Biomedical Sciences, Salzburg University of Applied Sciences, Urstein Süd 1, 4512 Puch bei Hallein, Austria

applications in consumer products and industry (Wang et al. 2016; Laux et al. 2018). During the production process, workers are potentially exposed to high silica NP concentrations in the air, mainly during the packing process after production of fumed silica prepared by a pyrolysis method as well as of colloidal silica NPs prepared by a polymerization process (Oh et al. 2014). Generally, amorphous silica NPs are considered as non-toxic especially when ingested (van der Zande et al. 2014), although the impact on the immune system in the gut needs to be further investigated (Winkler et al. 2016, 2017). However, there are numerous studies which document the potential of silica NPs to induce adverse effects in vivo when inhaled (Murugadoss et al. 2017) and in various in vitro models of pulmonary toxicity employing different human lung cells (Murugadoss et al. 2017) including our own studies with epithelial cells (Panas et al. 2013, 2014) and macrophages (Panas et al. 2013; Marquardt et al. 2017; Fritsch-Decker et al. 2018). The underlying mechanisms of toxicity are, however, still insufficiently understood (Murugadoss et al. 2017; Haase et al. 2017).

Silica nanoparticles are categorized as surface active materials which perturb the integrity of biological targets such as cellular membranes (Gebel et al. 2014; Lynch et al. 2014). Formation of a protein corona on the silica surface by adsorption of serum proteins suppresses adverse effects in multiple cell types (Al-Rawi et al. 2011; Ruh et al. 2012; Lesniak et al. 2012; Neagu et al. 2017). Thus, for intravenous administration of silica NPs, as intended in the field of nanomedicine, e.g., for drug delivery (Nyström and Fadeel 2012; Song et al. 2017), the presence of a protein corona needs to be considered. In contrast, for inhalation toxicology, in vitro experiments in the absence of serum proteins much better reflect the outcome in vivo as recently demonstrated for 18 different nanomaterials tested in short-term inhalation studies (Wiemann et al. 2016).

In the present study, we analyzed the effects of two silica NP preparations: Aerosil®200, commercially available silica NPs produced by flame synthesis (SiO₂-12 nm) and colloidal SiO₂-50 nm NPs produced by Stöber synthesis in A549 human alveolar epithelial cells. These cells are widely used as a model for the human alveolar surface, because they retain typical properties of type II cells such as secretion of pulmonary surfactant (Blank et al. 2006). Type II cells differentiate into type I cells which cover most of the alveolar surface. Previously, we documented the induction of cytotoxicity and pro-inflammatory responses in A549 cells upon exposure to SiO₂-12 nm NPs which were abrogated in the presence of serum (Panas et al. 2013). Here, we extended our analysis and included in addition to pyrogenic nanosilica colloidal silica as their biocompatibility might differ due to, e.g., altered surface properties. As read-outs, we employed high-throughput methods which speed up hazard ranking of nanomaterials (Delaval et al. 2017), i.e., we

analyzed the mode of cell death in more detail by microscopy at the single cell level. In addition, the regulation of the pro-inflammatory cytokine IL-8 was studied not only by monitoring the amount of the mRNA and protein but also transcriptional activation was investigated. To this end, we used transgenic A549 cells with an integrated luciferase reporter driving expression under the control of a minimal human IL-8 promoter. Furthermore, we performed detailed dose–response experiments to assess a possible correlation of cytotoxicity and the onset of pro-inflammatory responses. As the protein corona prevents toxicity of silica NPs, the impact of serum proteins was further investigated, specifically also with respect to cellular uptake. Finally, in the lung, not only epithelial cells encounter NPs upon inhalation, but also macrophages are essential target cells and are critically involved in pathophysiological processes. Therefore, all endpoints, i.e., cell death, pro-inflammatory response and cellular uptake, as well as the effect of the protein corona, were examined in a murine RAW264.7 macrophage cell line, which is widely used in the field of particle toxicology (Fritsch-Decker et al. 2011, 2018).

Materials and methods

Materials

Dulbecco's modified Eagle's medium (DMEM), medium supplements, phosphate-buffered saline without calcium and magnesium (PBS) and Hank's balanced salt solution (HBSS) were obtained from Life Technologies (Frankfurt, Germany). Fetal bovine serum (FBS Gold) was supplied from PAA (Cölbe, Germany). The lactate dehydrogenase (LDH) cytotoxicity assay kit was purchased from Roche (Mannheim, Germany) and the AlamarBlue reagent from AbD Serotec (Düsseldorf, Germany). Hoechst 33242 (Hoechst), propidium iodide (PI), and standard laboratory chemicals were supplied by Sigma-Aldrich (Taufkirchen, Germany). Aerosil®200 (SiO₂-12 nm) was kindly provided by Evonik (Frankfurt, Germany). SiO₂-50 nm and rhodamine-labeled SiO₂-50 nm particles were purchased from micro-mod Partikeltechnologie (Rostock, Germany).

Particle characterization

For determining the particle size distribution by dynamic light scattering (DLS) as well as the zeta potential, a 1 mg/mL stock suspension in deionized water was prepared with all particles. The suspension made with SiO₂-12 nm powder was shortly vortexed and probe sonified with 30 strokes, 50% cycle duty, output control: 8 (Branson Sonifier 250, Schwäbisch Gmünd, Germany). SiO₂-50 nm NP suspensions were only vortexed, not sonified. The stock suspensions were

further diluted either in deionized H₂O, in pure DMEM or in DMEM with 1 or 10% FBS. The samples were then analyzed either directly (0 h) or after incubation at 37 °C and 5% CO₂ for 24 h immediately after vortexing using the Zetasizer Nano ZS (Malvern Instruments Ltd., Herrenberg, Germany) at 25 °C and data was processed by the Malvern Zetasizer Nano software. For measurements, a scattering angle of 173°, viscosity of 0.8872 cP and refractive index for SiO₂ NPs of 1.46 were selected. As the presence of a second peak (due to the presence of serum proteins) with a size of 8 nm ± 0.9 nm in samples containing FBS distorts artificially the size distribution of NPs (i.e., towards lower mean diameters), the main peak mean intensity is shown in Table S1b. Due to the high conductivity of the cell culture media which leads to corrosion of the electrodes (also in accordance with the information provided by the manufacturer), the zeta potential was assessed in water.

Particles were tested for endotoxin with the chromogenic endpoint Limulus Amebocyte Lysate (LAL) assay (Lonza, Basel, Switzerland), as there is no interference of silica NPs with this method (Smulders et al. 2012). Particle suspensions of 1 mg/mL in deionized water were centrifuged at 20,800×g for 10 min and the supernatants were tested according to the instructions of the manufacturer. The result for each particle type was below the lower limit of quantification of the test (0.1 EU/mL). It was therefore excluded that endotoxin contributed to the biological responses of the test cells.

For the pyrogenic SiO₂-12 nm, we previously reported that trace impurities were only detected for Ni (0.1 ppm) and Cu (0.2 ppm) which are not of toxicological concern (Mülhopt et al. 2018). For the colloidal silica NPs produced by Micromod (SiO₂-50 nm and rhodamine-SiO₂-50 nm), no data are available. However, for similar sized colloidal silica NPs, which were also prepared by Stöber synthesis, trace contaminants were below 67 ppm with Ca and Na as main elements (Mülhopt et al. 2018).

Preparation of particle suspensions for cell treatment

All particle dilutions were prepared freshly by first preparing a 1 mg/mL stock suspension in deionized water as described above. This stock solution was used to prepare different concentrations in pure medium or in medium containing FBS before adding to the cells. For pre-coating of particles, a 100 µg/mL NP solution was incubated in H₂O containing 10% FBS and incubated for 1 h at 37 °C. After centrifugation at 18,000×g at 20 °C for 40 min, the supernatant was discarded, the pellet washed with H₂O and centrifuged again at 18,000×g at 20 °C for 20 min. This pellet was resuspended in DMEM without FBS.

Cell culture and particle treatment

A549, a human alveolar type II-like cell line, was obtained from American Type Culture Collection (ATCC-No. CCL-185, Rockville, MD). The cells were grown in DMEM supplemented with 10% FBS, 2 mM L-glutamine, 100 µg/mL penicillin, and 100 U/mL streptomycin and split every 3–4 days. A549-IL8-luc reporter cells were grown in complete DMEM which was additionally supplemented with 0.5 g/L G418 sulfate. These cells are stably transfected with an expression vector encoding luciferase under the control of a minimal promoter region of the human *Cxcl8* gene (Oostingh et al. 2008).

For experiments, the cells were seeded into 96- or 24-well tissue culture plates 1 day before. The cell culture medium was removed and replaced with half the volume of the required test medium (DMEM ± FBS). Then, the second half of the final volume of the respective medium containing particles (double of the final concentration) was added to the cells, which were exposed for the indicated time periods to 0–100 µg/mL of pyrogenic or colloidal nanosilica. The final volume was 100 µL per well in 96-well plates and 626 µL per well in 24-well plates. After treatment, the cell culture plates were centrifuged at 300×g for 5 min and aliquots of the supernatants were removed for analysis of LDH release and the remainder was stored at –20 °C for later cytokine detection. The cells were analyzed for mitochondrial activity by AlamarBlue reduction or for luciferase activity in case of the A549-IL8-luc cells.

LDH release assay

LDH release into the supernatant medium is an indicator of plasma membrane rupture and thus for late apoptotic or necrotic cell death. LDH was analyzed in the supernatant medium using the cytotoxicity detection kit (Roche, Mannheim, Germany) as described previously (Dilger et al. 2016) according to the manufacturer's instructions. The optical density was measured with the microplate reader VERSAmax and the software package SoftMaxPro (Molecular Devices, Ismaning, Germany) at 450 nm. The relative amount of released LDH was normalized to the total amount of LDH of control cells which were completely lysed with 0.1% Triton X-100.

AlamarBlue assay

Intact cells convert the blue resazurin into the pink resorufin which is an indicator of intact function of mitochondrial dehydrogenases. Loss of AlamarBlue reduction indicates loss of metabolic activity. The cell culture medium was replaced by 10% (v/v) AlamarBlue in HBSS and incubated for 2 h. The resorufin fluorescence was detected with a

fluorescence microplate reader (MWG Biotech, Ebersberg, Germany) at 580 nm excitation and 620 nm emission wavelength. The fluorescence intensities of the samples were normalized to the non-treated control cells grown in the indicated media, respectively. In Panas et al. (Panas et al. 2013), we have shown previously that silica nanoparticles neither interfere with the LDH nor the AlamarBlue assay.

Microscopy-based determination of cell counts, apoptosis and necrosis

For microscopic assays, 1×10^4 A549 cells were seeded per well of 96-well plates and exposed to particles on the next day. Directly after exposure, the cells were incubated with 0.3 $\mu\text{g/mL}$ Hoechst and 0.25 $\mu\text{g/mL}$ PI at 37 °C and 5% CO_2 for 30 min. Subsequently, four images per well were acquired using the automated fluorescence microscope IX81 (Olympus, Germany) with a tenfold objective. Automated image analysis was carried out using the Olympus Scan[®] analysis software. The total number of cells was determined by counting the Hoechst-stained nuclei. The individual Hoechst signal intensities in combination with the PI staining were used to discriminate between the different stages of cell death. Whilst Hoechst can penetrate both viable and dead cells, PI can only enter cells with a damaged membrane. After classification of the detected cells into the different modes and stages of cell death (early or late apoptosis and necrosis), the total numbers of viable and dead cells as well as the percentage distribution of dead cells into the different stages of cell death were calculated and displayed [for further details see also (Hansjosten et al. 2018)].

Luciferase assay

The A549-IL8-luc cells were washed two times with $\text{PBS-Ca}^{2+}/\text{-Mg}^{2+}$ before the addition of 90 μL 1 \times luciferase lysis reagent (Promega, Mannheim, Germany) into each well of a 24-well plate. The plates were frozen at -20 °C for a minimum of 1 day. After thawing, the lysates were transferred into 1.5 mL tubes and centrifuged at $20,000\times g$ at 4 °C for 5 min. The supernatants were collected and 20 μL was transferred into a white 96-well plate. The luciferase signal was detected with the Victor Light 1420 luminometer (Perkin Elmer, Rodgau-Jügesheim, Germany) after adding freshly prepared luciferin according to the protocol from Promega (Mannheim, Germany).

Enzyme-linked immunosorbent assay (ELISA)

ELISA assays are frequently performed to assess the pro-inflammatory properties of nanomaterials (Piret et al. 2017). Secretion of interleukin-8 (IL-8) and tumor necrosis factor-alpha (TNF-alpha) were analyzed as described previously

(Diabaté et al. 2011; Fritsch-Decker et al. 2018) using the specific OptEIA ELISA kits according to the manufacturer's instructions (BD Biosciences, Heidelberg, Germany).

Detection of rhodamine-labeled SiO_2 -50 nm NPs

Microscopy images were acquired as described above. The fluorescence intensity (FI) of the rhodamine channel was extracted as described (Mane et al. 2018) and analyzed with NIH ImageJ software. The FI of each cell was expressed by the background-corrected total cell fluorescence (CTCF). 30 cells in 1 image were evaluated for control and each treatment group.

Transmission electron microscopy (TEM)

TEM analysis of particle-treated cells was performed as described earlier in Panas et al. (2013). Briefly, the cells were seeded on Transwell inserts (Corning no. 3412, 24 mm polycarbonate membranes with 0.4 μm pores). After treatment with particles, the cells were fixed with 1.25% glutaraldehyde, 2% paraformaldehyde, 0.1% NaN_3 in 0.1 M PIPES buffer (pH 7.0) for at least 24 h, post-fixed with 0.5% osmium tetroxide and stained with 2% uranyl acetate. After dehydration, the cells were embedded in Epon (Polysciences, Eppelheim, Germany), cut into ultrathin sections and imaged with a Zeiss TEM (EM 910, Oberkochen, Germany).

Statistical analysis

Results are expressed as means \pm SEM or means \pm SD. The significance of difference between two mean values was assessed by the Student's *t* test. A *p* value < 0.05 was considered to be statistically significant.

Results

Particle characterization

Here we investigated pyrogenic and colloidal nanosilica representing two main classes of engineered silica nanomaterials. Specifically, we used SiO_2 -12 nm NPs (trade name Aerosil[®]200) which were produced by flame synthesis and SiO_2 -50 nm NPs which were prepared by the Stöber synthesis (Stöber et al. 1968). The nominal particle size and specific surface area (SSA) of the SiO_2 -12 nm NPs were provided by the manufacturer as 12 nm and 200 ± 25 m^2/g , respectively. Previously, we used transmission electron microscopy (TEM) to study the size distribution, morphology and aggregation of Aerosil[®]200. SiO_2 -12 nm NPs are nearly spherical with variable primary particle sizes and form larger aggregates possibly

due to sintering (Panas et al. 2013). The measured primary particle size of the SiO₂-50 nm NPs is 55 ± 7 nm as determined by TEM analysis and the calculated SSA is 55 m²/g (Table S1a). For studies on cellular uptake, we also included rhodamine-labeled colloidal silica NPs (rhodamine–SiO₂-50 nm) and determined a primary particle size of 65 ± 7 nm and a SSA of 46 m²/g. Dynamic light scattering measurements (Table S1b) showed that the hydrodynamic size of the plain SiO₂-12 nm NPs suspended directly in cell culture medium (DMEM) is increased in the presence of serum in accordance with our previous findings (Panas et al. 2013). The hydrodynamic size of FBS-pre-coated SiO₂-12 nm NPs also increased significantly indicating that protein adsorption promotes agglomeration of silica NPs. SiO₂-50 nm NPs have been shown to be nearly monodispersed when suspended in water (Al-Rawi et al. 2011) or DMEM (Panas et al. 2014). When colloidal SiO₂-50 nm NPs were dispersed in the presence of FBS, a slight increase in size could be detected (Table S1b) which is much less pronounced as observed for the pyrogenic SiO₂-12 nm NPs. However, pre-incubation with FBS and subsequent resuspension in DMEM further aggravated agglomeration possibly, due to enhanced particle interactions facilitated by several rounds of centrifugation. Finally, we measured the zeta potential of the selected NPs (Table S1c). All silica particles are, as expected, negatively charged. Interestingly, also after centrifugation and resuspension, the zeta potential does not change significantly indicating that NPs are not really affected by the purification method. Furthermore, coating of the NPs only slightly reduces the zeta potential.

Silica NPs trigger membrane rupture only in the absence of serum in A549 cells

Both types (pyrogenic and colloidal) of silica NPs induced LDH release in dependence of dose and in the absence of serum after 24 h incubation of A549 lung epithelial cells (Fig. 1a, b). Cytotoxicity after exposure to SiO₂-12 nm NPs became apparent already at 10 µg/mL, while for SiO₂-50 nm NPs the threshold dose was increased to 50 µg/mL. In the presence of 10% FBS, LDH release in response to silica NPs was largely suppressed.

Silica NPs provoke apoptotic cell death only in the absence of serum in A549 cells

Both types of silica NPs reduced the number of viable cells in dependence of dose and again only in the absence of serum after 24 h incubation (Fig. 2a, c). Further analysis of the specific mode of cell death induced by silica NPs revealed typical signs of late apoptosis, i.e., condensed and fragmented chromatin, cell shrinkage and disturbed membrane integrity (Fig. S1). Again, as observed above for the release of LDH (Fig. 1), cytotoxicity induced by pyrogenic SiO₂-12 nm NPs was more pronounced. As reported previously by us for murine RAW264.7 macrophages (Marquardt et al. 2017), we also observed the appearance of vacuoles in NP-treated A549 cells (Fig. S1). In RAW264.7 cells, these vacuoles detected in the brightfield images were further characterized as autophagosomes by electron microscopy which are typical hallmarks of autophagy. Interestingly, formation of vacuoles in A549 cells also correlated with the absence of cell death at the single cell level suggesting that silica NPs induce an adaptive and cyto-protective autophagy response in A549 cells as well.

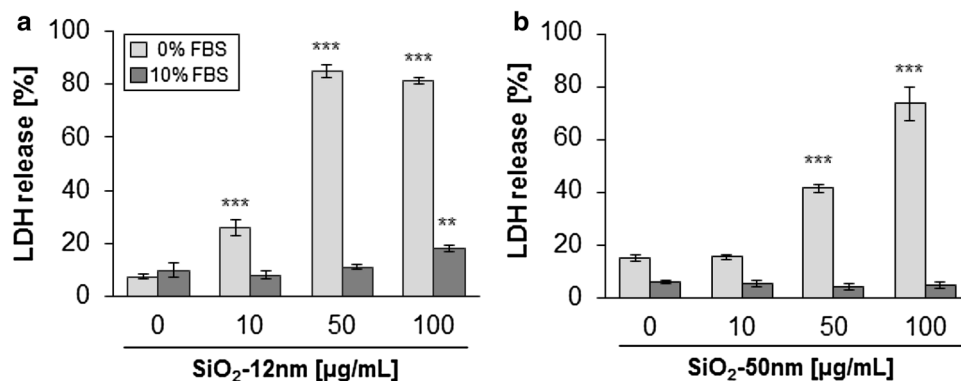


Fig. 1 SiO₂-12 nm NPs (Aerosil®200) and SiO₂-50 nm induced LDH release in dependence of concentration and presence of serum. A549 cells were treated with 10, 50 and 100 µg/mL SiO₂-12 nm (a) and SiO₂-50 nm NPs (b) without or with 10% serum for 24 h and the supernatants were analyzed for LDH release. For the positive control

untreated cells were lysed with Triton X-100. Results are presented relative to the Triton control (100%). The values are means obtained from three independent experiments performed in duplicate ± s.e.m.. **p* < 0.05, ***p* < 0.01, ****p* < 0.001 in comparison to cells not treated with particles

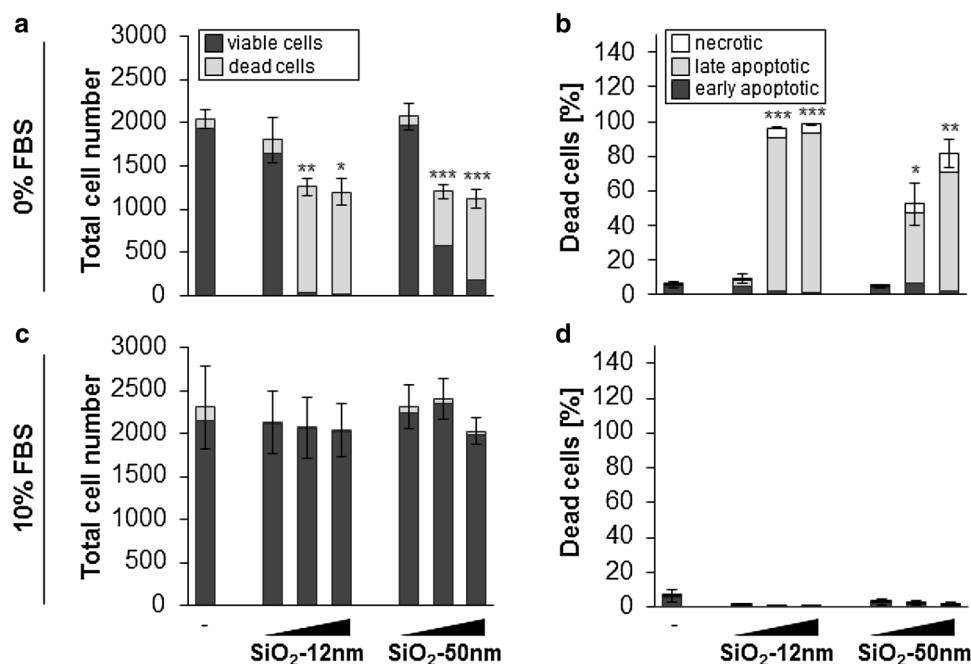


Fig. 2 Silica NPs reduce the number of viable cells and provoke cell death in the absence, but not in the presence of serum. A549 cells were treated with 0, 10, 50 and 100 µg/mL SiO₂-12 nm and SiO₂-50 nm NPs without (**a, b**) or with 10% serum (**c, d**) for 24 h. The cells were stained with Hoechst and PI and analyzed by automated high-throughput microscopy as described in the methods section. **a, c** The total cell number divided into living and dead cells

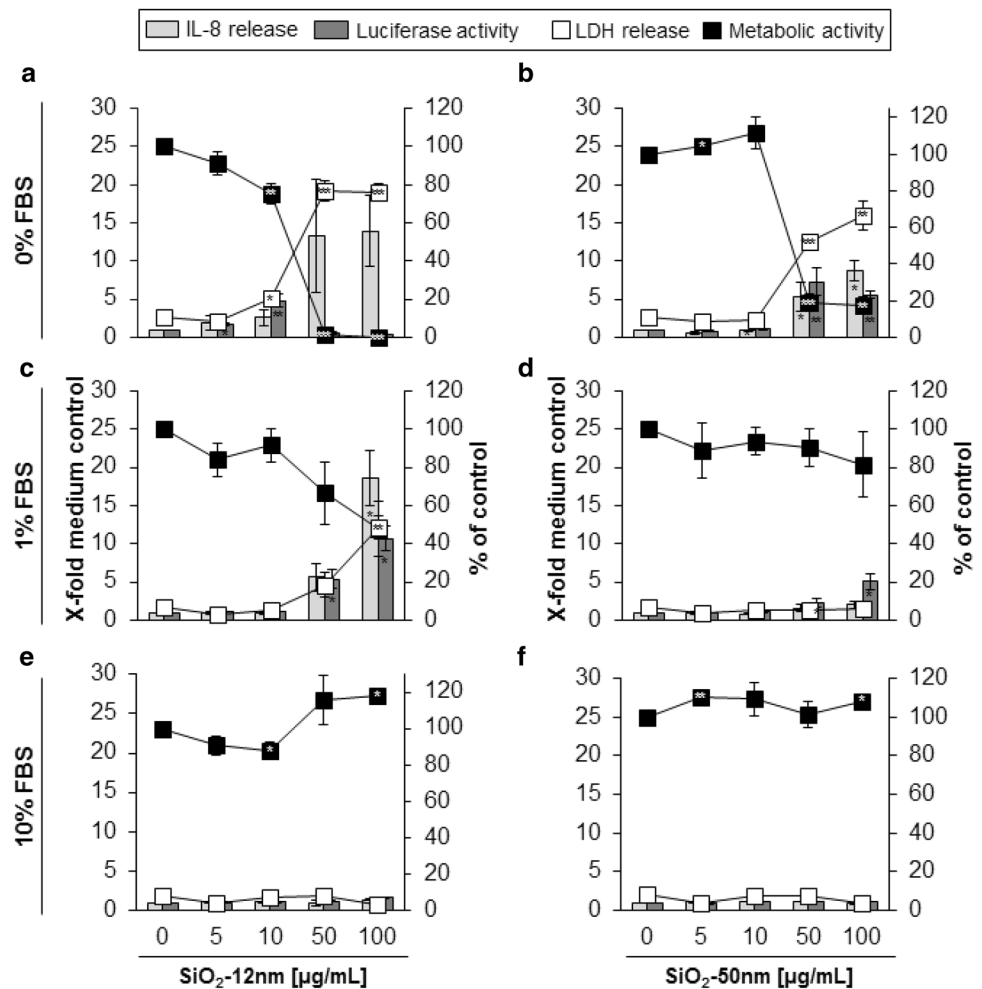
without and with 10% serum, respectively. **b, d** The percentage of dead cells relative to the total cell number divided into the different classes of cell death as indicated. Data show mean values of four independent experiments carried out with four replicates. The error bars are s.e.m. values related to the total cell number (**a, c**) or the amount of dead cells (**b, d**). * $p < 0.05$, ** $p < 0.01$, *** $p < 0.001$ in comparison to cells not treated with particles

Silica NP-induced cytotoxicity in A549 cells correlates with transcriptional activation and release of the pro-inflammatory chemokine IL-8

In previous studies, we showed that SiO₂-12 nm NPs enhanced the mRNA levels and secretion of IL-8 in A549 cells at a dose (50 µg/mL) which was also cytotoxic (Panas et al. 2013). Here, we performed detailed dose–response experiments to address a possible correlation of cytotoxicity (as detected by reduced metabolism and enhanced LDH release) and the release of the IL-8 protein. Furthermore, we used A549 cells with a stably transfected luciferase reporter under the control of a minimal human IL-8 promoter (A549-IL8-luc) to assess transcriptional activation. In addition, we included colloidal SiO₂-50 nm NPs and compared the responses to those induced by pyrogenic SiO₂-12 nm NPs. Finally, we investigated the effects of different serum concentrations (1 and 10% FBS, respectively) on NP actions on the different read-outs. Both silica NPs induced luciferase activity as well as release of the cytokine IL-8 in dependence of dose, in the absence of serum (Fig. 3a, b). Since SiO₂-12 nm NPs were highly toxic at 50 and 100 µg/mL and initiated cell lysis, luciferase activity could no longer be detected, as the enzyme is lost in the supernatant. However, secretion of IL-8 protein could still be observed (Fig. 3a), presumably because IL-8 is already produced and released

before membrane rupture occurs. The less toxic SiO₂-50 nm NPs also induced luciferase activity as well as IL-8 secretion, yet with reduced efficiency (Fig. 3b). Clearly, the onset of IL-8 transcription and IL-8 release correlated with the appearance of cytotoxic effects, i.e., reduced metabolism and membrane leakage. Also in the presence of 1% FBS, transcriptional activation and secretion of IL-8 could be detected after exposure to SiO₂-12 nm NPs (Fig. 3c). However, the dose response was shifted towards higher NP concentrations and as toxicity was less pronounced, transcriptional activation and release of IL-8 could simultaneously be detected. In case of SiO₂-50 nm NPs, 1% serum was already sufficient to almost completely suppress all responses. At 10% FBS, luciferase activity and IL-8 secretion were not detectable for both silica NPs, which correlated well with the absence of toxicity (Fig. 3e, f). In conclusion, cytotoxicity, i.e., cell lysis and reduction of metabolic activity provoked by silica NPs precedes transcriptional activation and release of IL-8 and is suppressed by increasing levels of serum.

Fig. 3 SiO₂ NP-induced cytotoxicity and reduction of metabolic activity correlates with the onset of transcriptional activation and release of IL-8. A549-IL8-luc cells were treated with 0, 5, 10, 50 and 100 µg/mL SiO₂-12 nm NPs and SiO₂-50 nm NPs in medium without (a, b) or with 1% (c, d) and 10% (e, f) serum for 24 h. For the positive control, untreated cells were lysed with Triton X-100. The supernatants were analyzed for LDH release and secreted IL-8. Cells were assessed for AlamarBlue reduction before cell lysis and luciferase activity was determined in the lysates. The right y axes present LDH release relative to the Triton control (100%) and AlamarBlue reduction relative to the untreated control (100%), respectively. The left y axes present IL-8 release and luciferase activity as *x*-fold of the untreated controls, respectively. The values are means obtained from three independent experiments performed in duplicate ± s.e.m. **p* < 0.05, ***p* < 0.01, ****p* < 0.001 in comparison to cells not treated with particles



Colloidal and pyrogenic silica NPs are similarly potent to promote toxic effects in A549 cells when the specific surface area dose is used as a metric

As silica NPs are surface active materials which interact with biological interfaces, the specific particle surface area (SSA, cm² at a defined mass or volume) is inversely correlated with the diameter, i.e., the SSA increases linearly with the reciprocal decrease in particle size. Hence, the calculated difference in SSA for the 12 and 50 nm silica NPs is indeed roughly fourfold (Table S1a). Deposition kinetics over 24 h are similar for both particles as calculated previously (Panaset al. 2014). Therefore, the SSA dose per cell layer surface area (cm²/cm²) was used as a metric to plot dose–response curves for the different endpoints assessed. Indeed, LDH release and metabolic activity correlate well with the specific surface area dose of the two types of silica NPs (Fig. 4a–c). Also, the release of IL-8 and transcriptional activation of the IL-8 promoter were similarly regulated by both silica NPs, although, as expected, at higher doses of

SiO₂-12 nm NPs luciferase activities sharply declined due to the high cytotoxicity of these particles as discussed above (Fig. 4d, e).

For a better comparison of the dose–responses according to different metrics, we calculated the EC₅₀ values (effective concentration either for the nominal mass concentration (µg/mL) or SSA dose (cm²/cm²), respectively, at which 50% of the maximal effect is observed) for the two types of silica NPs and for all endpoints (Table 1). EC₅₀ values for the surface area dose are very similar between the two silica particles for all endpoints (number of living cells, LDH release, metabolic activity, IL-8 release and transcription), while the EC₅₀ values for the nominal concentration are significantly higher for the SiO₂-50 nm NPs due to the approximately fourfold lower specific surface area (Table S1a).

In essence, the conventional approach to plot dose–responses related to the nominal concentration in the exposure media suggested increased toxicity of smaller silica NPs. In contrast, when the specific surface area is employed as a metric, both colloidal and pyrogenic silica NPs are equally effective.

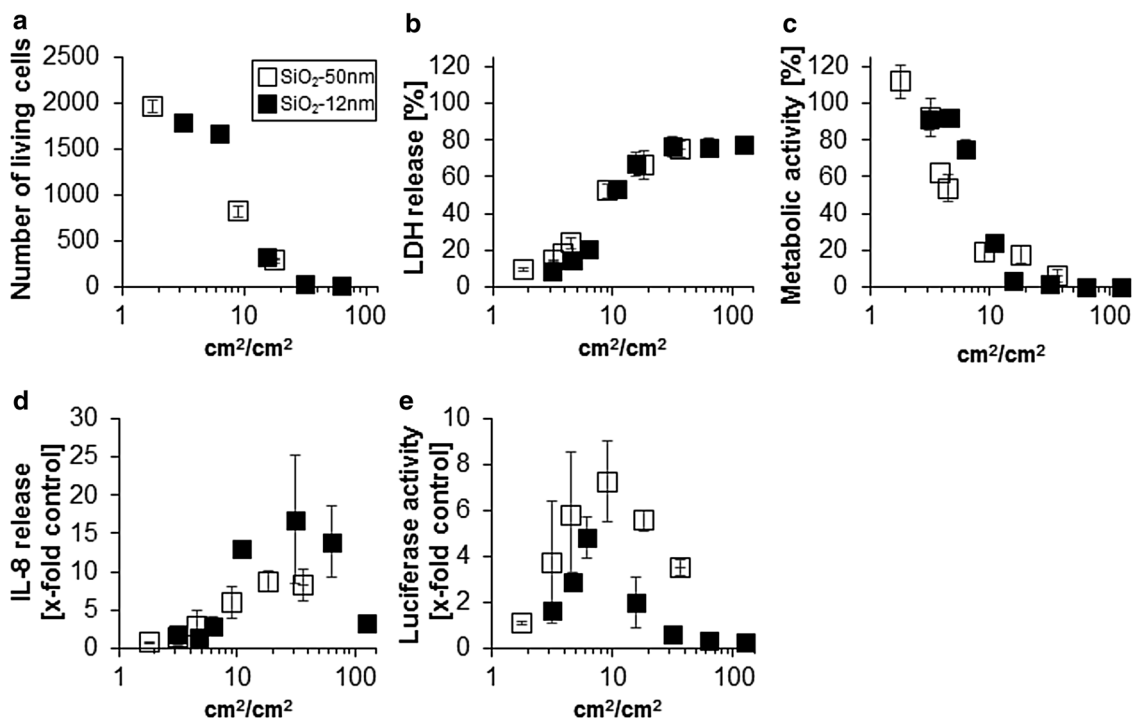


Fig. 4 Colloidal and pyrogenic silica NPs are equally potent to induce toxicity when considering the specific surface area dose as a metric. A549 (a) and A549-IL8-luc cells (b–e) cells were treated with different concentrations of SiO₂-12 nm and SiO₂-50 nm NPs in medium without serum for 24 h. **a** Cells were stained with Hoechst and PI and analyzed by automated fluorescence microscopy. The supernatants were analyzed for LDH release (b) and secreted IL-8 (d). The cells were assessed for AlamarBlue reduction (c) before lysis and thereafter for luciferase activity (e). For the LDH assay, the untreated

cells were lysed with Triton X-100 to obtain a positive control. LDH release is presented relative to the Triton control (100%) and Alamar-Blue reduction relative to the untreated control (100%). IL-8 release and luciferase activity are presented as x-fold of the untreated controls. All results are plotted against the specific surface area dose per cell area (cm²/cm², logarithmic scale) for the two silica particles. Results represent means ± s.e.m. from at least three independent experiments performed in quadruplicates

Table 1 EC₅₀ values of silica NPs administered to A549 cells and expressed as surface area dose (SD) and mass dose (MD)

| | SiO ₂ -12 nm | | SiO ₂ -50 nm | |
|---------------------|---|-----------------------------|---|-----------------------------|
| | EC ₅₀ SD (cm ² /cm ²) | EC ₅₀ MD (µg/mL) | EC ₅₀ SD (cm ² /cm ²) | EC ₅₀ MD (µg/mL) |
| Cytotoxicity | 8.5 | 13.5 | 8.7 | 47.9 |
| LDH release | 9.2 | 14.7 | 9.7 | 53.7 |
| Metabolic activity | 7.5 | 12.0 | 8.2 | 45.2 |
| IL-8 release | 9.8 | 15.7 | 9.6 | 52.7 |
| Luciferase activity | 5.6 | 9.0 | 3.8 | 20.8 |

Pre-coating of silica NPs with serum abrogates toxicity but enhances cellular uptake in A549 cells

Cells in the presence of serum might be more competent to adapt to stress induced by silica NPs and hence toxicity is reduced compared to exposures in the absence of serum. Alternatively, serum proteins could adsorb to the surface of silica NPs and thus inhibit interactions with cellular

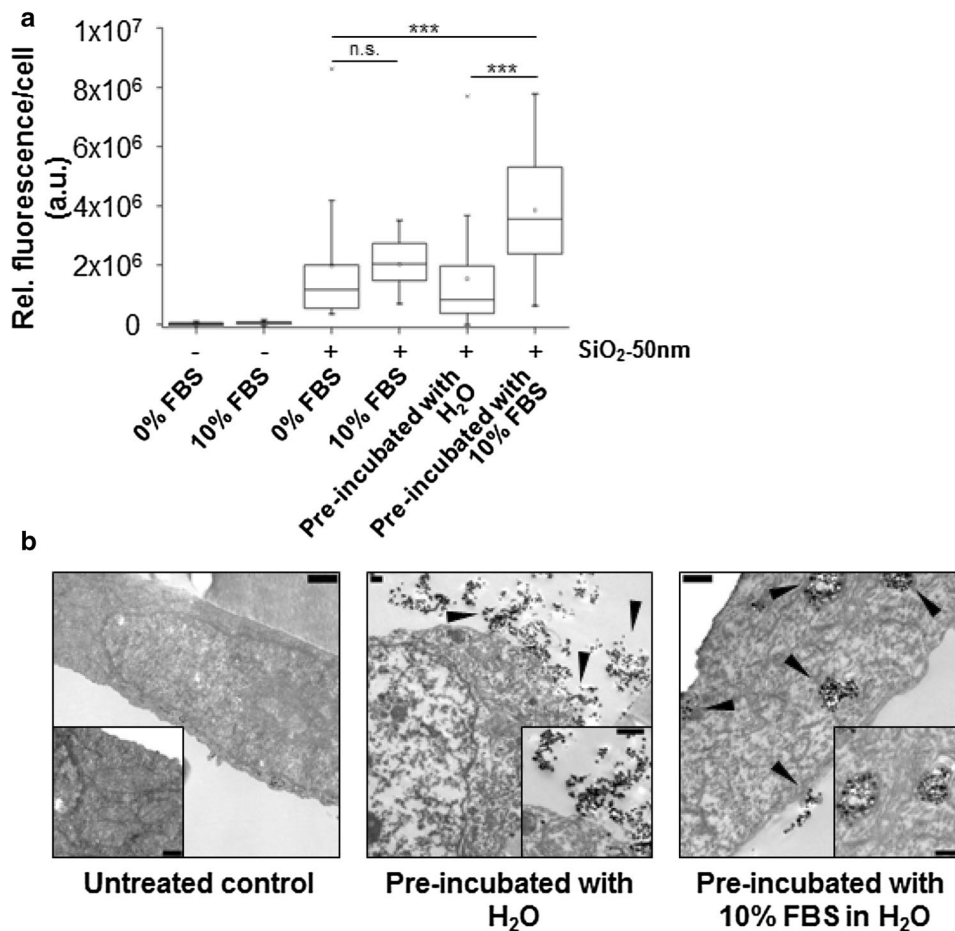
targets, such as membranes and thereby reduce or entirely suppress toxicity. In previous studies and in line with the latter hypothesis, silica NPs with a pre-adsorbed hard protein corona are non-toxic when exposed to A549 cells cultivated in media without serum (Panas et al. 2013). To this end, particles were incubated in H₂O with 10% FBS for 1 h at 37 °C, pelleted, washed in H₂O to remove unbound proteins and resuspended in DMEM without serum. After such a procedure, only proteins with a high binding affinity are bound (aka the hard protein corona), whereas loosely associated proteins (aka soft protein corona) are lost (Kokkinopoulou et al. 2017). In extension of our previous work, we now can also demonstrate that not only the cytotoxicity of pyrogenic but also colloidal silica NPs is suppressed by pre-formation of a hard protein corona (Fig. S2).

Next, we assessed the impact of the protein corona on cellular uptake. Therefore, rhodamine-labeled SiO₂-50 nm NPs were incubated in medium with (10% FBS) or without serum (0% FBS) to visualize and quantify uptake of particles. Surprisingly, large numbers of particle agglomerates could be detected on top of, but also adjacent to cells in the

absence of serum (Fig. S3a). However, in the presence of serum, particles were confined to the perinuclear region and no agglomerates could be detected. Indeed, washing of cultures exposed in serum-free medium could remove to a large extent particle agglomerates (Fig. S4). Similar results were obtained for serum pre-coated rhodamine-labeled SiO_2 -50 nm NPs (Fig. S3b). Although, as summarized in Table S1b, the size of rhodamine-labeled silica NPs in media is smaller in the absence of serum (about 64 nm) compared to the presence of serum (about 94 nm), particles seem to agglomerate at the bottom of the cell culture well. Similar observations were made previously for silica NPs which agglomerated on polymer coated but not on plain glass cover slips (Landgraf et al. 2017). This opposed behavior was also seen in case of serum pre-coated silica NPs which are on average 81 nm in the absence and about 247 nm in the presence of adsorbed proteins. Nevertheless, without pre-adsorbed proteins, a strong agglomeration of NPs was evident. Yet again, in the presence of a protein corona particles more stringently co-localized with the cells, although some agglomerates were still visible. Hence, for quantification of particle uptake, cultures were washed after exposure to remove agglomerates and the

mean fluorescence intensity per cell was evaluated at the single cell level to exclude background signals from the extracellular space (Fig. 5a). When cells were treated with particles in the presence of serum, a tendency of higher particle uptake compared to the conditions without serum could be noted, yet the difference did not reach statistical significance. The impact of the protein corona became more obvious when cells were exposed to pre-coated NPs. Clearly, the fluorescence intensity per cell was increased when NPs with a pre-formed protein corona were investigated. To corroborate these findings, we also performed TEM experiments to image cells and NPs at higher resolution (Fig. 5b). In line with the fluorescence imaging approach, we could not spot NPs without a pre-formed protein corona inside A549 cells, but some were attached to the outer cellular surface. In contrast, in the presence of a protein corona, NPs were localized inside the cells.

Fig. 5 The protein corona facilitates uptake of rhodamine-labeled SiO_2 -50 nm NPs into A549 cells. **a** A549 cells were exposed to 50 $\mu\text{g}/\text{mL}$ rhodamine-labeled SiO_2 -50 nm NPs in the presence or absence of FBS or to NPs with a pre-formed protein corona in medium without FBS for 24 h. A549 cells were stained with Hoechst and cellular uptake was analyzed by automated high-throughput microscopy as described under “Materials and methods”. **b** A549 cells were exposed to 50 $\mu\text{g}/\text{mL}$ rhodamine-labeled SiO_2 -50 nm NPs with a pre-formed protein corona in serum-free medium for 6 h and then prepared for TEM analysis as described under Methods. Black arrows indicate SiO_2 -50 nm NPs. Bars (overview and inset) = 500 nm



The protein corona suppresses cytotoxicity and a pro-inflammatory response but enhances particle uptake after exposure of RAW264.7 macrophages to silica NPs

In the lung, not only epithelial cells but also macrophages encounter NPs upon inhalation. We therefore studied the impact of the protein corona on silica NP-induced effects in RAW264.7 macrophages. Similar to the results obtained with A549 cells and in accordance with our previous studies (Marquardt et al. 2017), exposure of RAW264.7 macrophages to pyrogenic SiO₂-12 nm NPs in serum-free medium triggered apoptosis. In the presence of serum, however, the reduction of cell counts and enhanced cell death was abrogated (Figs. S5a, b). Moreover, pyrogenic silica NPs promoted the release of the pro-inflammatory cytokine TNF- α in the absence of serum, as has been reported previously (Fritsch-Decker et al. 2018). More important, this pro-inflammatory response could also be inhibited by the addition of serum (Fig. S5c). We also repeated this set of experiments with colloidal SiO₂-50 nm NPs. Again, as shown for pyrogenic silica NPs, colloidal particles reduced the number of viable cells and initiated apoptosis (Fig. 6a) as well as a pro-inflammatory response (Fig. 3). All adverse reactions could be prevented by incubation of particles in the presence of serum. Finally, the uptake of rhodamine-labeled particles was monitored in cells incubated in the presence or absence of serum. As discussed above in case of A549 cells, agglomerates of NPs were visible in serum-free medium and particles associated with the cell membrane but did not enter the cells (Fig. S6a). On the contrary, NPs were efficiently incorporated when serum was present in the medium. Pre-coating of particles with a protein corona also promoted uptake in serum-free medium, whereas in its absence particles again stick to the cell surface (Fig. S6b). Quantification of cellular fluorescence confirmed the increased particle uptake due to the presence of serum (Fig. 6c). TEM experiments visualize the attachment of particles to the cell membrane when no protein corona was adsorbed, whereas particles with a pre-formed corona readily entered the cells (Fig. 6d). In summary, RAW264.7 macrophages behave very similar to A549 epithelial cells, i.e., both types of silica NPs induce cytotoxicity and pro-inflammatory responses which are alleviated by adsorption of serum to the particle surface.

Discussion

Previously, we demonstrated that the presence of FBS in cell culture media abolished the cytotoxic and pro-inflammatory activity of pyrogenic SiO₂-12 nm NPs in lung epithelial cells (A549) and macrophages (RAW 264.7) (Panas et al. 2013). Incubation of SiO₂-12 nm NPs in media complemented with

FBS leads to the formation of a protein corona, which is dominated by the most abundant serum proteins, i.e., components of the complement system, immunoglobulins and albumin (Casals et al. 2010; Ruh et al. 2012). Therefore, we pre-coated SiO₂-12 nm NPs with FBS or simply bovine serum albumin, purified the NP–protein complexes and added them to A549 cells cultured in the absence of serum. Again, the toxic effects induced by pyrogenic silica NPs in the absence of a protein corona were completely suppressed when NPs were pre-coated with serum proteins (Panas et al. 2013). Here, we extended our analysis and investigated also colloidal SiO₂-50 nm NPs, which similarly to pyrogenic SiO₂-12 nm NPs, induced cell death in HeLa human carcinoma cells only in the absence but not in the presence of serum (Al-Rawi et al. 2011). Detailed dose response experiments in A549 cells demonstrated that both types of silica NPs triggered cytotoxicity as evidenced by the release of LDH and the reduction of metabolic activity and number of viable cells. The mode of cell death was further characterized and is reminiscent of apoptosis. Also, both types of silica NPs promoted a pro-inflammatory response as monitored by the release of IL-8. Interestingly, normalization of the dose response curves to the specific NP surface area indicated a similar potency of both types of particles to induce toxic effects. This is in agreement with a number of in vitro and in vivo studies which have shown that cytotoxicity of insoluble NPs better correlates with the particle surface area dose than with the particle mass dose (Donaldson et al. 2002; Stoeger et al. 2007). Thus, as silica NPs are surface active materials, adsorption of a protein corona abolishes toxicity as shown in our experiments where silica NPs were either added to cells in the presence of serum or were pre-coated with FBS. Noteworthy, in vitro experiments with alveolar macrophages cultivated in the absence of serum have been demonstrated to predict the short-term inhalation toxicity in vivo for 18 different nanomaterials including nanosilica (Wiemann et al. 2016). Upon inhalation, NPs are not covered by serum proteins and encounter macrophages and lung epithelial cells which are covered by the lung lining fluid mostly comprised of surfactant (primarily phospholipids) and a small amount of proteins. Therefore, exposure of cells in vitro in the presence of high levels of serum proteins (10% FBS) do not closely mimic the physiological conditions in the lung. Even in the presence of 1% serum, we could still observe toxicity of SiO₂-12 nm NPs in A549 cells in line with previous results obtained with human colon carcinoma cells (Gehrke et al. 2013). These findings suggest that the ratio of the specific particle surface area and concentration of proteins in the biological environment will critically determine the adverse outcome. Interestingly, suppression of a pro-inflammatory response, i.e., release of IL-8 in lung epithelial cells by serum proteins despite an increased cellular uptake has also been observed for amine-modified

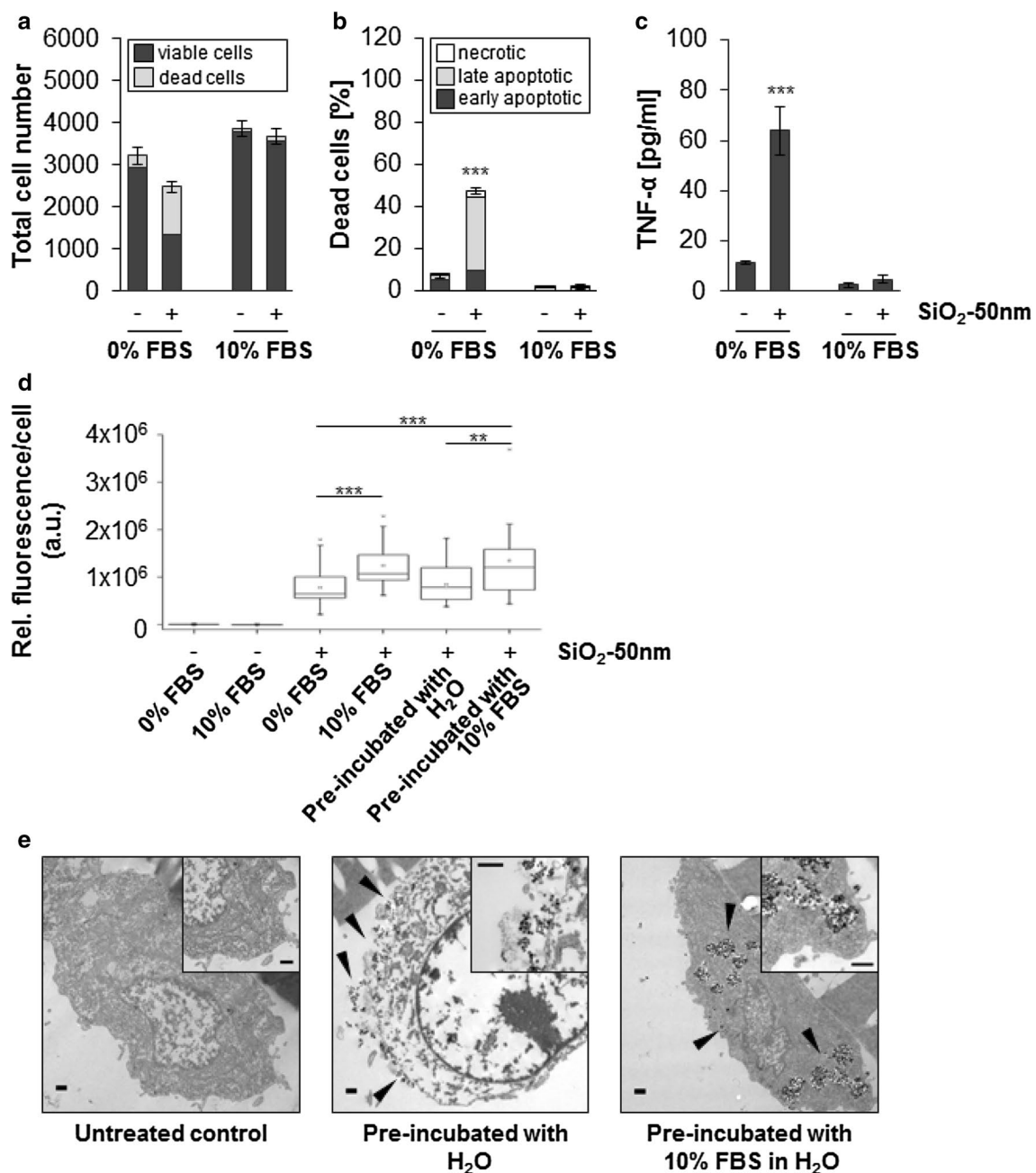


Fig. 6 Colloidal SiO₂ NPs reduce the number of viable cells, provoke cell death and induce the release of TNF α in RAW264.7 cells in the absence but not in the presence of serum. **a–c** RAW264.7 cells were exposed to 50 μ g/mL SiO₂-50 nm without (0%) or with (10%) FBS for 6 h. The cells were stained with Hoechst and PI and analyzed by automated high-throughput microscopy as described in the methods section. **a** The total cell number divided into living and dead cells. **b** The percentage of dead cells relative to the total cell number divided into the different classes of cell death as indicated. Data show mean values of three independent experiments carried out with four replicates. * p < 0.05, ** p < 0.01, *** p < 0.001 in comparison to cells not treated with particles. **c** The amount of TNF-alpha in the supernatant

medium was quantified by ELISA. Results are given as means \pm SD from 2 to 3 independent experiments each carried out in duplicate (** p < 0.01, *** p < 0.001 in comparison to the respective untreated controls). **d** Macrophages were exposed to 50 μ g/mL rhodamine-labeled SiO₂-50 nm NPs in the presence or absence of FBS or to NPs with a pre-formed protein corona in medium without FBS for 24 h. Cells were stained with Hoechst and cellular uptake was analyzed by automated high-throughput microscopy as described under Methods. **e** Cells were exposed to 50 μ g/mL SiO₂-50 nm NPs with a pre-formed protein corona in serum-free medium for 6 h and then prepared for TEM analysis as described under Methods. Black arrows indicate SiO₂-50 nm NPs. Bars (overview and inset) = 500 nm

tania NPs (Vranic et al. 2017). Therefore, the impact of the protein corona needs to be investigated more systematically in the future to identify physico-chemical properties of various nanomaterials ultimately determining adverse effects and biokinetics in vitro and in vivo. Furthermore, as mentioned above, in the conducting airways NPs will encounter different surface layers with distinct composition and hence the impact of surfactant and mucus found in the respective lung tissues (i.e., alveoli and bronchi) on the toxicity of nanosilica needs to be investigated in the future. It should be noted that our experiments were designed to better understand the principles of nanosilica/cell interaction without a focus on risk assessment and the dose investigated here does not necessarily mimic a tissue delivered dose in humans. As nanosilica is not yet applied in the clinics for, e.g., pulmonary drug delivery, we used concentrations documented for superparamagnetic iron oxide nanoparticles which are used as contrast agents for imaging. Plasma concentrations in patients are about 30–40 µg/mL (Shaw et al. 2008) and therefore we used a similar dose range. However, for occupational exposure concentrations are much lower (Paur et al. 2011), although in the literature 50 µg/mL is nevertheless often used to simulate cumulative exposure over many years or to take into account the strong accumulation of NPs at the branching points of the airways in the lung (Phalen et al. 2006). Our findings also re-emphasize that for hazard assessment and ranking of different nanomaterials in vitro assays should not be performed in the presence of high levels of serum as this suppresses adverse effects. Beyond its direct relevance for improved toxicity testing, one could envisage that for intended pulmonary delivery of NPs adsorption of a protein corona might prevent potential adverse effects and hence improve biocompatibility. Apart from typical features of cell death, the appearance of vacuoles, which is a typical hallmark of autophagy, was also evident, specifically in viable A549 cells. Indeed, induction of autophagy by exposure to silica NPs has also been observed by others and could be detected by monodansylcadaverine staining in A549 cells accompanied by enhanced expression of the autophagy genes ATG 12 and beclin (Nowak et al. 2014). Induction of autophagy seems not confined to a particular cell type, as exposure of RAW264.7 macrophages to silica NPs provoked classical hallmarks of autophagy as evidenced by TEM and accumulation of the protein LC3-II (Herd et al. 2011; Marquardt et al. 2017). Promotion of autophagy is an adaptive and cytoprotective response and enhances survival of RAW264.7 macrophages after exposure to silica NPs (Marquardt et al. 2017). As visualized at the single cell level in RAW264.7 macrophages and now also in A549 cells, features of cell death and autophagy are mutually exclusive and dependent on the dose of silica NPs.

In addition to cytotoxicity, another important endpoint of silica toxicity is a pro-inflammatory response. Interestingly,

inflammation and cell death are tightly connected and dying cells promote inflammatory signaling (Zitvogel et al. 2010). Here, we monitored the release of IL-8 from A549 cells and simultaneously monitored cytotoxicity in detailed dose–response experiments. Clearly, the onset of IL-8 release coincides with the occurrence of cytotoxicity. The regulation of cytokines is very complex and involves transcriptional and post-transcriptional control of the relevant mRNA but is also modulated at the translational, post-translational and secretory level (Gaestel et al. 2009). As the amount of the IL-8 mRNA as well as the release of the IL-8 protein is enhanced after exposure to SiO₂-12 nm NPs (Panas et al. 2013) we addressed in the present study the transcriptional activation of the IL-8 promoter. Both types of silica NPs potently activated gene expression driven by a minimal promoter region encompassing 250 bp of the human IL-8 promoter (Oostingh et al. 2008). In this region, the binding sites for the transcription factors AP-1, C/EBP and NF-κB are located which are key regulators of IL-8 gene expression (Roebuck 1999). Recently, we reported activation of AP-1 and its upstream regulatory mitogen-activated protein kinase (MAPK) pathway upon exposure to silica NPs in RAW264.7 macrophages (Fritsch-Decker et al. 2018). Similarly, activation of the MAPK cascade by nanosilica occurs in A549 cells (Panas et al. 2013, 2014). Hence, further experiments are warranted to interrogate the role of AP-1 and MAPKs but also of NF-κB in the transcriptional activation of IL-8 after exposure to silica NPs.

So far, the molecular initiating event to trigger cell death and pro-inflammatory signaling remains elusive. Possibly, the pristine silica surface interacts with certain proteins and/or phospholipids in the cell membrane to perturb membrane integrity ultimately resulting in cell death but also to initiate signaling events. Deleterious interactions of silica NPs with cellular membranes are known since quite some time, however, the exact molecular details are still poorly defined (Pavan et al. 2013; Iler 1981). Furthermore, it will be of interest to explore the coupling of cytotoxicity and pro-inflammatory signaling at the single cell level, as both processes might interact in the same or alternatively in adjacent cells.

Finally, we explored the uptake of labeled silica NPs in the presence of serum or a pre-formed protein corona into A549 cells and RAW264.7 macrophages. Adsorption of serum proteins promotes internalization of silica NPs, as confirmed by light and electron microscopy. This outcome is at odds with earlier experiments where, based on flow cytometry, in the absence of serum, an increased amount of silica NPs associated with A549 cells were detected and hence an enhanced uptake was postulated (Lesniak et al. 2012). However, in the absence of FBS silica NPs adhere to the outer cell membrane even as larger aggregates as observed in our light microscopy analysis, but also in TEM

studies by Lesniak et al. The primary size of 50 nm colloidal silica NPs is only slightly increased to approximately 64 nm in the absence of serum and further enhanced in the presence of serum to roughly 94 nm owing to the formation of a soft protein corona as also reported previously by others (Lesniak et al. 2012; Kokkinopoulou et al. 2017). Nevertheless, on top of the cell monolayer and the cell culture dish, silica NPs agglomerated in serum-free medium and thus increased amounts of particles were associated with cells. These agglomerates impede proper quantification of particle uptake if cultures were not washed properly before fluorescence was measured. Specifically, flow cytometry cannot distinguish between associated and internalized NPs and thus imaging needs to be performed at the single cell level to reliably monitor uptake.

Purification of NP protein complexes mainly retains the tightly bound proteins also known as the hard protein corona. In the medium, however, a soft corona including low affinity binding proteins is formed. The soft corona is for technical limitations poorly defined and comparisons between the biological impact of the soft versus the hard protein corona are scarce. Interestingly, the presence of a hard protein corona is sufficient to promote cellular uptake in both cell types and experiments with a pre-adsorbed corona recapitulate the situation in the presence of serum where a more complex soft corona is formed. More studies are warranted to systematically address the role of the soft and hard protein corona on the biological activity of NPs. As protein coating of the NPs only slightly reduces the zeta potential (Table S1c), increased uptake in the presence of a protein corona is unlikely explained by a different surface charge but rather directly mediated by adsorbed proteins. Exactly which proteins of the soft or hard protein corona mediate particle uptake via which receptor is still in most cases unknown. To complicate matters further, the protein corona supports but also inhibits cellular uptake of NPs in RAW264.7 macrophages as exemplified for nanosilica in this study and for polystyrene NPs by others (Kokkinopoulou et al. 2017). Thus, more rigorous imaging approaches should screen multiple particle and cell types for the effect of the protein corona on cellular uptake to potentially link physico-chemical properties of NPs to protein adsorption and cellular internalization.

In conclusion, the present work highlights the critical role of the pristine silica NP surface to promote adverse effects in lung epithelial cells and macrophages. The nano–bio-interface, which is critical in this context, is comprised of the silica surface interacting with cellular membranes which are dependent on dose results in cytotoxicity and pro-inflammatory responses. Formation of a protein corona suppresses toxicity, presumably by inhibition of detrimental interactions with sensitive membrane constituents. On the other hand, the protein corona supports cellular uptake. Our

results are consistent with the observed pulmonary toxicity, where silica NPs encounter bio-liquids with low amounts of proteins. In case of exposure in the presence of high levels of serum proteins, as in case of injection into the blood stream, silica NPs are rather biocompatible and are cleared by macrophages.

Acknowledgements RL and AMW were funded by a grant of the Federal Institute for Risk Assessment (BfR), Germany (BfR-ZEBET-1329-475) which is greatly acknowledged.

Compliance with ethical standards

Conflict of interest The authors declare that they have no conflicts of interest.

Ethical approval This article does not contain any studies with human participants or animals performed by any of the authors.

References

- Al-Rawi M, Diabaté S, Weiss C (2011) Uptake and intracellular localization of submicron and nano-sized SiO₂ particles in HeLa cells. *Arch Toxicol* 85:813–826
- Blank F, Rothen-Rutishauser BM, Schurch S, Gehr P (2006) An optimized in vitro model of the respiratory tract wall to study particle cell interactions. *J Aerosol Med* 19:392–405
- Casals E, Pfaller T, Duschl A, Oostingh GJ, Puentes V (2010) Time evolution of the nanoparticle protein corona. *ACS Nano* 4:3623–3632
- Delaval M, Wohlleben W, Landsiedel R, Baeza-Squiban A, Boland S (2017) Assessment of the oxidative potential of nanoparticles by the cytochrome c assay: assay improvement and development of a high-throughput method to predict the toxicity of nanoparticles. *Arch Toxicol* 91:163–177
- Diabaté S, Bergfeldt B, Plaumann D, Übel C, Weiss C (2011) Anti-oxidative and inflammatory responses induced by fly ash particles and carbon black in lung epithelial cells. *Anal Bioanal Chem* 401:3197–3212
- Dilger M, Orasche J, Zimmermann R, Paur HR, Diabaté S, Weiss C (2016) Toxicity of wood smoke particles in human A549 lung epithelial cells: the role of PAHs, soot and zinc. *Arch Toxicol* 90:3029–3044
- Donaldson K, Brown D, Clouter A, Duffin R, MacNee W, Renwick L, Tran L, Stone V (2002) The pulmonary toxicology of ultrafine particles. *J Aerosol Med* 15:213–220
- Fritsch-Decker S, Both T, Mülhopt S, Paur HR, Weiss C, Diabaté S (2011) Regulation of the arachidonic acid mobilization in macrophages by combustion-derived particles. *Part Fibre Toxicol* 8:23
- Fritsch-Decker S, Marquardt C, Stoeger T, Diabaté S, Weiss C (2018) Revisiting the stress paradigm for silica nanoparticles: decoupling of the anti-oxidative defense, pro-inflammatory response and cytotoxicity. *Arch Toxicol* 92:2163–2174
- Gaestel M, Kotlyarov A, Kracht M (2009) Targeting innate immunity protein kinase signalling in inflammation. *Nat Rev Drug Discov* 8:480–499
- Gebel T, Foth H, Damm G, Freyberger A, Kramer PJ, Lilienblum W, Röhl C, Schupp T, Weiss C, Wollin KM, Hengstler JG (2014) Manufactured nanomaterials: categorization and approaches to hazard assessment. *Arch Toxicol* 88:2191–2211
- Gehrke H, Frühmesser A, Pelka J, Esselen M, Hecht LL, Blank H, Schuchmann HP, Gerthsen D, Marquardt C, Diabaté S, Weiss

- C, Marko D (2013) In vitro toxicity of amorphous silica nanoparticles in human colon carcinoma cells. *Nanotoxicology* 7:274–293
- Haase A, Dommershausen N, Schulz M, Landsiedel R, Reichardt P, Krause BC, Tentschert J, Luch A (2017) Genotoxicity testing of different surface-functionalized SiO₂, ZrO₂ and silver nanomaterials in 3D human bronchial models. *Arch Toxicol* 91:3991–4007
- Hansjosten I, Rapp J, Reiner L, Vatter R, Fritsch-Decker S, Peravali R, Palosaari T, Joossens E, Gerloff K, Macko P, Whelan M, Gilliland D, Ojea-Jimenez I, Monopoli MP, Rocks L, Garry D, Dawson K, Röttgermann PJF, Murschhauser A, Rädler JO, Tang SVY, Gooden P, Belinga-Desaunay MA, Khan AO, Briffa S, Guggenheim E, Papadiamantis A, Lynch I, Valsami-Jones E, Diabaté S, Weiss C (2018) Microscopy-based high-throughput assays enable multi-parametric analysis to assess adverse effects of nanomaterials in various cell lines. *Arch Toxicol* 92:633–649
- Herd HL, Malugin A, Ghandehari H (2011) Silica nanoconstruct cellular toleration threshold in vitro. *J Control Release* 153:40–48
- Iler R (1981) The surface chemistry of amorphous synthetic silica - interaction with organic molecules in an aqueous medium. In: Dunnom D (ed) Health effects of synthetic silica particulates, STP38665S. ASTM International, West Conshohocken, pp 3–29
- Kokkinopoulou M, Simon J, Landfester K, Mailänder V, Lieberwirth I (2017) Visualization of the protein corona: towards a biomolecular understanding of nanoparticle-cell-interactions. *Nanoscale* 9:8858–8870
- Landgraf L, Nordmeyer D, Schmiel P, Gao Q, Ritz S, Gebauer S, Graß S, Diabaté S, Treuel L, Graf C, Rühl E, Landfester K, Mailänder V, Weiss C, Zellner R, Hilger I (2017) Validation of weak biological effects by round robin experiments: cytotoxicity/biocompatibility of SiO₂ and polymer nanoparticles in HepG2 cells. *Sci Rep* 7:4341
- Laux P, Tentschert J, Riebeling C, Braeuning A, Creutzenberg O, Epp A, Fessard V, Haas KH, Haase A, Hund-Rinke K, Jakubowski N, Kearns P, Lampen A, Rauscher H, Schoonjans R, Störmer A, Thielmann A, Mühle U, Luch A (2018) Nanomaterials: certain aspects of application, risk assessment and risk communication. *Arch Toxicol* 92:121–141
- Lesniak A, Fenaroli F, Monopoli MP, Aberg C, Dawson KA, Salvati A (2012) Effects of the presence or absence of a protein corona on silica nanoparticle uptake and impact on cells. *ACS Nano* 6:5845–5857
- Lynch I, Weiss C, Valsami-Jones E (2014) A strategy for grouping of nanomaterials based on key physico-chemical descriptors as a basis for safer-by-design NMs. *Nano Today* 9:266–270
- Mane SR, Hsiao IL, Takamiya M, Le D, Straehle U, Barner-Kowollik C, Weiss C, Delaittre G (2018) Intrinsically fluorescent, stealth polypyrazoline nanoparticles with large stokes shift for in vivo imaging. *Small* 14:e1801571
- Marquardt C, Fritsch-Decker S, Al-Rawi M, Diabaté S, Weiss C (2017) Autophagy induced by silica nanoparticles protects RAW264.7 macrophages from cell death. *Toxicology* 379:40–47
- Mülhopt S, Diabaté S, Dilger M, Adelhelm C, Anderlohr C, Bergfeldt T, Gomez dIT, Jiang Y, Valsami-Jones E, Langevin D, Lynch I, Mahon E, Nelissen I, Piella J, Puentes V, Ray S, Schneider R, Wilkins T, Weiss C, Paur HR (2018) Characterization of nanoparticle batch-to-batch variability. *Nanomaterials* (Basel) 8:311
- Murugadoss S, Lison D, Godderis L, van den Brule S, Mast J, Brassinne F, Sebaili N, Hoet PH (2017) Toxicology of silica nanoparticles: an update. *Arch Toxicol* 91:2967–3010
- Neagu M, Piperigkou Z, Karamanou K, Engin AB, Docea AO, Constantin C, Negrei C, Nikitovic D, Tsatsakis A (2017) Protein corona: critical issue in immune nanotoxicology. *Arch Toxicol* 91:1031–1048
- Nowak JS, Mehn D, Nativo P, Garcia CP, Gioria S, Ojea-Jimenez I, Gilliland D, Rossi F (2014) Silica nanoparticle uptake induces survival mechanism in A549 cells by the activation of autophagy but not apoptosis. *Toxicol Lett* 224:84–92
- Nyström AM, Fadeel B (2012) Safety assessment of nanomaterials: implications for nanomedicine. *J Control Release* 161:403–408
- Oh S, Kim B, Kim H (2014) Comparison of nanoparticle exposures between fumed and sol-gel nano-silica manufacturing facilities. *Ind Health* 52:190–198
- Oostingh GJ, Schmittner M, Ehart AK, Tischler U, Duschl A (2008) A high-throughput screening method based on stably transformed human cells was used to determine the immunotoxic effects of fluoranthene and other PAHs. *Toxicol In Vitro* 22:1301–1310
- Panas A, Marquardt C, Nalcaci O, Bockhorn H, Baumann W, Paur HR, Mülhopt S, Diabaté S, Weiss C (2013) Screening of different metal oxide nanoparticles reveals selective toxicity and inflammatory potential of silica nanoparticles in lung epithelial cells and macrophages. *Nanotoxicology* 7:259–273
- Panas A, Comouth A, Saathoff H, Leisner T, Al-Rawi M, Simon M, Seemann G, Dössel O, Mülhopt S, Paur HR, Fritsch-Decker S, Weiss C, Diabaté S (2014) Silica nanoparticles are less toxic to human lung cells when deposited at the air-liquid interface compared to conventional submerged exposure. *Beilstein J Nanotechnol* 5:1590–1602
- Paur HR, Fissan H, Rothen-Rutishauser B, Teeguarden JG, Diabaté S, Aufderheide M, Kreyling W, Cassee FR, Hänninen O, Kasper G, Riediker M, Schmid O (2011) In-vitro cell exposure studies for the assessment of nanoparticle toxicity in the lung—a dialogue between aerosol science and biology. *J Aerosol Sci* 42:668–692
- Pavan C, Tomatis M, Ghiazza M, Rabolli V, Bolis V, Lison D, Fubini B (2013) In search of the chemical basis of the hemolytic potential of silicas. *Chem Res Toxicol* 26:1188–1198
- Phalen RF, Oldham MJ, Nel AE (2006) Tracheobronchial particle dose considerations for in vitro toxicology studies. *Toxicol Sci* 92:126–132
- Piret JP, Bondarenko OM, Boyles MSP, Himly M, Ribeiro AR, Benetti F, Smal C, Lima B, Potthoff A, Simion M, Dumortier E, Leite PEC, Balottin LB, Granjeiro JM, Ivask A, Kahru A, Radauer-Preiml I, Tischler U, Duschl A, Saout C, Anguissola S, Haase A, Jacobs A, Nelissen I, Misra SK, Toussaint O (2017) Pan-European inter-laboratory studies on a panel of in vitro cytotoxicity and pro-inflammation assays for nanoparticles. *Arch Toxicol* 91:2315–2330
- Roebuck KA (1999) Regulation of interleukin-8 gene expression. *J Interferon Cytokine Res* 19:429–438
- Ruh H, Kühl B, Brenner-Weiss G, Hopf C, Diabaté S, Weiss C (2012) Identification of serum proteins bound to industrial nanomaterials. *Toxicol Lett* 208:41–50
- Shaw SY, Westly EC, Pittet MJ, Subramanian A, Schreiber SL, Weissleder R (2008) Perturbational profiling of nanomaterial biologic activity. *Proc Natl Acad Sci USA* 105:7387–7392
- Smulders S, Kaiser JP, Zuin S, Van Landuyt KL, Golanski L, Vanoirbeek J, Wick P, Hoet PH (2012) Contamination of nanoparticles by endotoxin: evaluation of different test methods. *Part Fibre Toxicol* 9:41
- Song Y, Li Y, Xu Q, Liu Z (2017) Mesoporous silica nanoparticles for stimuli-responsive controlled drug delivery: advances, challenges, and outlook. *Int J Nanomed* 12:87–110
- Stöber W, Fink A, Bohn E (1968) Controlled growth of monodisperse silica spheres in the micron size range. *J Colloid Interface Sci* 26:62–69
- Stoeger T, Schmid O, Takenaka S, Schulz H (2007) Inflammatory response to TiO₂ and carbonaceous particles scales best with BET surface area. *Environ Health Perspect* 115:A290–A291
- van der Zande M, Vandebriel RJ, Groot MJ, Kramer E, Herrera Rivera ZE, Rasmussen K, Ossenkoppele JS, Tromp P, Gremmer ER, Peters RJ, Hendriksen PJ, Marvin HJ, Hoogenboom RL, Peijnenburg AA, Bouwmeester H (2014) Sub-chronic toxicity study in

- rats orally exposed to nanostructured silica. *Part Fibre Toxicol* 11:8
- Vranic S, Gosens I, Jacobsen NR, Jensen KA, Bokkers B, Kermani-zadeh A, Stone V, Baeza-Squiban A, Cassee FR, Tran L, Boland S (2017) Impact of serum as a dispersion agent for in vitro and in vivo toxicological assessments of TiO₂ nanoparticles. *Arch Toxicol* 91:353–363
- Wang Y, Kalinina A, Sun T, Nowack B (2016) Probabilistic modeling of the flows and environmental risks of nano-silica. *Sci Total Environ* 545–546:67–76
- Wiemann M, Vennemann A, Sauer UG, Wiench K, Ma-Hock L, Landsiedel R (2016) An in vitro alveolar macrophage assay for predicting the short-term inhalation toxicity of nanomaterials. *J Nanobiotechnol* 14:16
- Winkler HC, Suter M, Naegeli H (2016) Critical review of the safety assessment of nano-structured silica additives in food. *J Nano-biotechnol* 14:44
- Winkler HC, Kornprobst J, Wick P, von Moos LM, Trantakis I, Schraner EM, Bathke B, Hochrein H, Suter M, Naegeli H (2017) MyD88-dependent pro-interleukin-1beta induction in dendritic cells exposed to food-grade synthetic amorphous silica. *Part Fibre Toxicol* 14:21
- Zitvogel L, Kepp O, Kroemer G (2010) Decoding cell death signals in inflammation and immunity. *Cell* 140:798–804

Publisher's Note Springer Nature remains neutral with regard to jurisdictional claims in published maps and institutional affiliations.